

# Brownian force noise from molecular collisions and the sensitivity of advanced gravitational wave observatories

R. Dolesi, M. Hueller, D. Nicolodi, D. Tombolato,\* S. Vitale, P. J. Wass,† and W. J. Weber  
*Dipartimento di Fisica, Università di Trento, and I.N.F.N., Gruppo di Trento, 38123 Povo (TN), Italy*

M. Evans, P. Fritschel, and R. Weiss  
*Massachusetts Institute of Technology, LIGO, Cambridge, MA 02139*

J. H. Gundlach, C. A. Hagedorn, and S. Schlamminger‡  
*Center for Experimental Nuclear and Particle Astrophysics, University of Washington, Seattle, WA 98195*

G. Ciani  
*Department of Physics, University of Florida, Gainesville, FL 32611*

A. Cavalleri  
*Istituto di Fotonica e Nanotecnologie, C.N.R.- Fondazione Bruno Kessler, 38123 Povo (TN), Italy*  
(Dated: November 6, 2018)

We present an analysis of Brownian force noise from residual gas damping of reference test masses as a fundamental sensitivity limit in small force experiments. The resulting acceleration noise increases significantly when the distance of the test mass to the surrounding experimental apparatus is smaller than the dimension of the test mass itself. For the Advanced LIGO interferometric gravitational wave observatory, where the relevant test mass is a suspended 340 mm diameter cylindrical end mirror, the force noise power is increased by roughly a factor 40 by the presence of a similarly shaped reaction mass at a nominal separation of 5 mm. The force noise, of order 20 fN/Hz<sup>1/2</sup> for  $2 \times 10^{-6}$  Pa of residual H<sub>2</sub> gas, rivals quantum optical fluctuations as the dominant noise source between 10 and 30 Hz. We present here a numerical and analytical analysis for the gas damping force noise for Advanced LIGO, backed up by experimental evidence from several recent measurements. Finally, we discuss the impact of residual gas damping on the gravitational wave sensitivity and possible mitigation strategies.

PACS numbers: 05.40.-a, 07.10.Pz, 07.30.-t, 95.55.Ym

## I. INTRODUCTION

The Brownian motion of a macroscopic test mass is a fundamental limit in many small force measurements, which ideally require a test mass (TM) to be free of stray forces, and thus a reference of purely inertial motion, except for any known and calibrated suspension forces. The power spectrum of the Brownian force noise acting on the TM is related to any source of mechanical dissipation, given by the mechanical impedance  $Z(\omega)$ , through the fluctuation-dissipation theorem

$$S_F(\omega) = 4k_B T \operatorname{Re}[Z(\omega)] = 4k_B T \operatorname{Re}\left(-\frac{F(\omega)}{v(\omega)}\right). \quad (1)$$

Gas damping in the molecular flow regime is known to produce viscosity proportional to the residual gas pressure,  $Z(\omega) = \beta \sim p[1-4]$ , with  $\beta$  referred to here as the gas damping coefficient. In the limit to which the collisions can be treated as independent impulses, the resulting Brownian force noise has a frequency independent spectrum. Residual gas force noise has recently been reconsidered in the context of gravitational experiments with geodesic-reference TM [5, 6]. In these and other experiments, the proximity of surrounding surfaces can significantly increase the gas damping, and thus the re-

sulting force noise, over that observed for the same TM in an infinite volume filled only with gas. This phenomenon, referred to here as proximity-enhanced gas damping, has also been observed and studied for MEMS oscillators, under the name of squeeze film damping [7, 8].

While there is a continuum of behavior between the free damping (infinite gas volume) limit and proximity damping, we will divide the total molecular impact force noise into these contributions,

$$S_F(\omega) = S_F^\infty + \Delta S_F(\omega). \quad (2)$$

$S_F^\infty = 4k_B T \beta^\infty$  is the noise for the TM in an infinite gas volume, while the excess  $\Delta S_F$  depends on the TM proximity to surrounding surfaces.

Though long unnoticed in experimental gravitation, proximity-enhanced gas damping has a straightforward physical explanation: motion of a TM, with characteristic dimension  $s$ , in the vicinity of another surface, at some small distance  $d$ , creates a transient squeezing of any residual gas in the gap between the two bodies. With the subsequent molecular flow out of the gap, there is an associated pressure drop, proportional to the molecular current, and thus a velocity dependent force. In an alternate picture, the Brownian force noise increases because of the correlation between repeated impacts of a molecule

on the TM as it stochastically moves along the gap. As the same random walk statistics govern the molecular flow down the channel, these two pictures – of dissipative flow and correlated collision impulses – are equivalent, as Eqn. 1 requires.

The grouping of repeated impulses into “macro-collisions” establishes a natural interaction (or correlation) time  $\tau$ , the typical time needed for random walk molecular diffusion out of the interbody gap. This creates a high frequency cutoff,  $\omega \approx \tau^{-1}$ , above which the force noise decreases. In terms of the macroscopic flow impedance picture, TM motion for  $\omega\tau \gg 1$  is too fast to allow molecular flow, with the real, dissipative, part of  $Z(\omega)$  decreasing to leave only the imaginary impedance of gas compression. We will return to these simple arguments later in the article for an approximate analytical model that is useful in interpreting the results of our study, for  $\Delta S_F$  and  $\tau$  in terms of the aspect ratio  $s/d$ .

Recent experimental studies [5, 6] place the physics of proximity-enhanced gas damping on a quantitative footing. These studies both measure the gas damping on the free oscillation of torsion pendulums, focusing on the low frequency range  $\omega\tau \ll 1$  where  $\beta$  is independent of frequency. The torsion pendulum inertial elements in these studies were a cubic TM inside a cubic enclosure and a rectangular plate in close proximity of a second parallel plate. The TM size-to-gap aspect ratios studied range from roughly 4 to 400. Both experiments observed a clear proximity excess in the gas damping, well beyond calculated values of  $\beta^\infty$ . These experiments will be discussed in Sec. IV.

Gas damping has been analyzed as a force noise source for terrestrial gravitational wave interferometers [3] but should be reconsidered for the next generation experiments, both for their stringent acceleration noise requirements and for the close proximity of TM to the surrounding apparatus. For Advanced LIGO [9, 10], the envisioned end mirror TM are right cylinders of fused silica with radius  $R = 17$  cm and length  $h = 20$  cm (mass  $M \approx 40$  kg). In an infinite gas volume, at  $T = 293$  K and pressure  $p = 2 \times 10^{-6}$  Pa of residual  $H_2$  gas ( $m_0 = 2$  amu), the molecular impact force noise, integrated over the entire cylindrical TM surface, would be [4]

$$\begin{aligned} S_F^\infty &= p(128\pi m_0 k_B T)^{1/2} R^2 \left(1 + \frac{h}{2R} + \frac{\pi}{4}\right) \\ &\approx \left[3.2 \text{ fN/Hz}^{1/2} \times \left(\frac{p}{2 \times 10^{-6} \text{ Pa}}\right)^{1/2}\right]^2. \end{aligned} \quad (3)$$

This free damping compares favorably with the Advanced LIGO target, which requires total force noise below  $40 \text{ fN/Hz}^{1/2}$  at frequencies near 30 Hz to reach a strain sensitivity of  $10^{-23}/\text{Hz}^{1/2}$  (equivalent to a TM acceleration noise of roughly  $1 \text{ fm/s}^2/\text{Hz}^{1/2}$ ). However, the original Advanced LIGO design includes cylindrical “reaction masses,” with the same radius and 13 cm length, facing the TM at a nominal separation  $d = 5$  mm (see

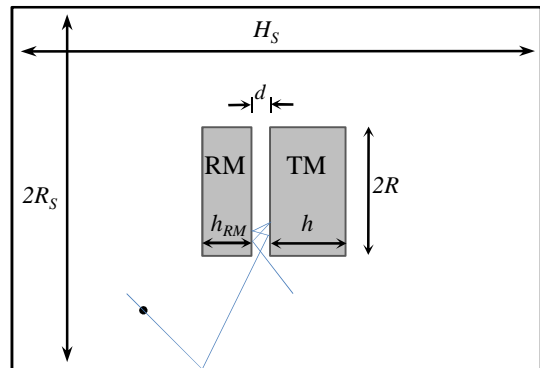


FIG. 1: Cartoon illustration of the Advanced LIGO experimental configuration studied and simulated here, seen perpendicular to the symmetry axes of the cylindrical test (TM) and reaction (RM) masses, with radii  $R = 17$  cm and heights  $h = 20$  cm and  $h_{RM} = 13$  cm. The gap  $d$ , nominally 5 mm for Advanced LIGO, is varied in the simulations. The simulated experimental enclosure, not shown to scale here, is a coaxial cylinder of radius  $R_S = 10R$  and length  $H_S = 11h + h_{RM} + d$ .

Fig. 1). The close reaction masses are needed for all four cavity mirror TM, for electrostatic force actuation and for compensating optical thermal lensing from TM laser heating. The relevant aspect ratio of  $2R/d \approx 70$  is well into the regime of proximity-enhanced gas damping, and thus the problem merits a thorough understanding.

In this article, we calculate the force noise and diffusion time using a numerical simulation of a molecule exchanging momentum with the TM mirrors in the Advanced LIGO geometry, as a function of the gap size (Section II). In Section III these results are compared with an approximate analytical model, which successfully explains the functional dependence of the excess force noise on gap size in terms of a simple random walk picture. In Section IV, the physics and simulation techniques of Secs. II and III are compared with experimental evidence from similar systems. Finally, in Section V we address the impact of gas damping force noise on the sensitivity of advanced gravitational wave detectors and discuss possible mitigation strategies. While the article focuses on the Advanced LIGO geometry, we will discuss design consideration for other advanced gravitational wave observatories in the conclusion.

As in previously cited experimental and numerical studies [4–6, 8], we consider completely inelastic molecular collisions with the TM, with subsequent immediate random reemission with a cosine angular distribution. The inelastic, diffuse scattering hypothesis is verified experimentally for spinning rotor pressure gauges and is the basis for their use as absolute pressure calibration standards [11, 12]. This also guarantees time reversal invariance and Maxwell-Boltzmann statistics in the gas phase (see Ref. [13]). The immediate reemission approximation is valid in the limit that the effective sticking time,  $\tau_{st}$ , is negligible compared to that needed to cross the gap be-

tween TM,  $\frac{d}{v_T}$ . This is justified for  $H_2$  and other possible gas species on the TM  $SiO_2$  surface at room temperature, based on the relevant adsorption potentials, in Appendix A. Finally, we treat the average gas pressure as uniform in the system, which requires that the gap pressure is not dominated by local outgassing from the test or reaction mass, which would cause a stable increase in the relevant local pressure. We return to these last two points in the conclusions.

## II. NUMERICAL STUDY OF BROWNIAN FORCE NOISE

We have performed Monte Carlo simulations to analyze the gas damping noise for the Advanced LIGO geometry. The simulations (following those performed in [5]) trace the trajectory of a gas molecule as it moves inside a large volume containing the cylindrical test mass and reaction mass. The molecular species is chosen to be  $H_2$  at room temperature, the dominant residual gas expected in the Advanced LIGO vacuum chamber, which sets the scale of momentum exchange upon impact and the time scale between collisions through the characteristic thermal velocity  $v_T \equiv \sqrt{k_B T/m} \approx 1100$  m/s. The volume enclosing the two cylinders, ideally infinite, is chosen to be a cylinder ten times larger, in both radius and length, than the volume envelope defined by the two cylinders and the intervening gap.

The simulation starts by random selection of a molecular position, from a uniform distribution in the available volume – including the gap but also the much larger, and thus more probable, space surrounding the cylinders – and velocity, from a Maxwell-Boltzmann distribution. The impacts with the walls are completely inelastic, with subsequent immediate random thermal reemission following a cosine angular distribution, independent of the incoming velocity, with the resulting gas distribution obeying Maxwell-Boltzmann statistics (the reemission distribution is given in Eqn. C1, as in Ref. [4]). At each collision with the TM – regardless of whether the molecule strikes on the TM surface facing the gap or on the opposing side or outer wall – the time and exchanged momentum vector are recorded. Simulations are run, for a single molecule, for a time  $T_0$  (in the range of  $10^{-6}$  - 10 s, chosen to abundantly cover the full range of the observed values of  $\tau$ ) and then repeated for many trials. Finally, the simulations have been performed as a function of gap  $d$  between the two cylinders, in the range from 100  $\mu\text{m}$  to 1 m.

One way to probe the simulation is to observe the statistical fluctuations of the total momentum  $\Delta q$  exchanged along the critical cylindrical symmetry axis in repetitions of the simulations of duration  $T_0$ . This allows simple extraction of the parameters describing the amplitude and spectral shape of the force noise. For a process with white force noise up to some high frequency rolloff associated with a time constant  $\tau$ , with  $S_F = \frac{S_{F_0}}{1+(\omega\tau)^2}$ ,

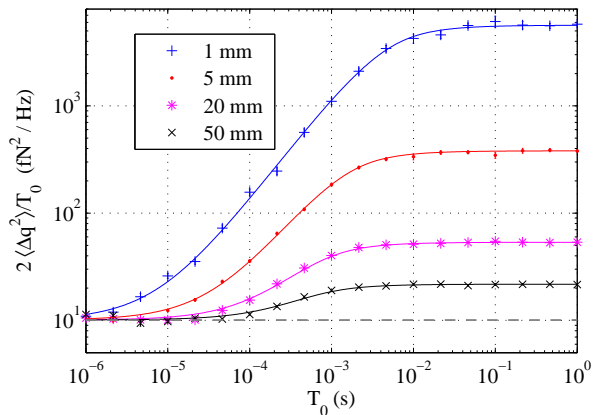


FIG. 2: Simulation data for the scatter in the total momentum  $\Delta q$  transferred to the TM in simulation time  $T_0$ , for several values of the intercylinder gap  $d$ , each fit to the model in Eqn. 6. The range of gaps studied represents aspect ratios ( $2R/D$ ) from nearly 7 to 340. The dashed gray line represents the prediction in the limit of infinite gap,  $S_F^\infty$ , which is recovered for very short simulation times. Data are scaled for a reference pressure  $p = 2 \times 10^{-6}$  Pa.

one can calculate (see Appendix B)

$$\langle(\Delta q)^2\rangle = \frac{S_{F_0}T_0}{2} \left( 1 - \frac{1 - \exp(-\frac{T_0}{\tau})}{\frac{T_0}{\tau}} \right), \quad (4)$$

with  $\langle(\Delta q)^2\rangle = \frac{S_{F_0}T_0}{2}$  in the limit  $T_0 \gg \tau$ .

In our simulations, we directly calculate the average scatter in  $\Delta q$  from the total momentum exchange in the different trials, typically calculating  $\langle(\Delta q)^2\rangle$  from groups of  $10^3$  (for the longer simulations) to  $10^6$  (shorter  $T_0$ ) single molecule experiments and then estimate the simulation uncertainty between 100 such groups. In a physical experiment with many non-interacting gas molecules,  $\langle(\Delta q)^2\rangle$ , and thus also the force noise power, is proportional to the number of molecules in the system, allowing us to scale our single molecule simulations to a given pressure (we choose  $2 \times 10^{-6}$  Pa as a reference pressure to put a relevant experimental scale to the data presented).

Figure 2 shows simulation data for  $\frac{2\langle(\Delta q)^2\rangle}{T_0}$  as a function of measurement time  $T_0$  for several values of the gap  $d$ . The data show a clear increase in force fluctuations with decreasing gap. The time dependence shows saturation for large  $T_0$ , as predicted by Eqn. 4 and which we can associate with  $\tau$ , but also a saturation to a nonzero value at short  $T_0$ , for which this simple model with a single high frequency rolloff does not account. This low- $T_0$  saturation has, however, a simple physical explanation: for  $T_0$  below roughly  $d/v_T$  – the time necessary for a molecule to cross the intercylinder gap, see Appendix C – a molecule will hit the TM at most once during the simulation. In this limit the simulation becomes blind to any correlation effects related to proximity, as for a cylindrical TM in an infinite volume. In fact, the low- $T_0$  saturation values shown in Fig. 2 converge, for different values

of  $d$ , to the infinite volume value,  $S_F^\infty$ . There would also be a natural time scale and associated high frequency rolloff relevant to the simulation in the single collision (or infinite volume) limit, but it corresponds to the single collision duration, which the simulation takes to be infinitesimal. These curves thus both confirm the infinite volume force noise prediction for short simulations and, in the longer simulations, indicate an increasing excess force noise for decreasing  $d$ .

We note that no excess force fluctuations are observed for the components orthogonal to the cylinder symmetry axis, for which the infinite volume limit of Ref. [4] is verified. The correlation in the force from successive impacts is only non-zero for the component normal to the surface, for which the direction of the impulse is always toward the test mass center, whereas the sign of the shear component of momentum exchange along an axis parallel to the surface is random. From a macroscopic damping standpoint, TM motion parallel to the reaction mass does not squeeze the gas between the two bodies, and thus creates no dissipative gas flow in the narrow gap.

With these results in mind, we modify the force noise model to

$$S_F(\omega) = S_F^\infty + \frac{\Delta S_{F_0}}{1 + (\omega\tau)^2}, \quad (5)$$

where  $\Delta S_{F_0}$  represents the excess low frequency force noise associated with the proximity effect. For each  $d$ , the curves in Fig. 2 are thus fitted to a model modified from Eqn. 4 to include the infinite volume limit,

$$\frac{2\langle(\Delta q)^2\rangle}{T_0} = S_F^\infty + \Delta S_{F_0} \left( 1 - \frac{1 - \exp(-T_0/\tau)}{T_0/\tau} \right), \quad (6)$$

with the total low frequency force noise  $S_{F_0}$  obtained in the limit  $T_0 \gg \tau$ ,

$$\lim_{T_0 \rightarrow \infty} \frac{2\langle(\Delta q)^2\rangle}{T_0} \equiv S_{F_0} = S_F^\infty + \Delta S_{F_0}. \quad (7)$$

This allows extraction of the free fit parameters corresponding to the low frequency force noise  $S_{F_0}$  and diffusion time  $\tau$ , which are plotted as a function of  $d$  in, respectively, Figs. 3 and 4 [28].

The Monte Carlo molecular dynamics simulation can also be probed by sampling the momentum exchange with the test mass in repeated time intervals to create a force time series, which can then be analyzed for the frequency dependent noise spectrum. Force noise spectra have been calculated using a 100  $\mu$ s sampling time – and thus well shorter than the relevant values of  $\tau$  – for a simulation of 10 seconds, which has been analyzed in overlapping 0.4 s windows, with averaging over roughly 25 statistically independent spectra. These data, displayed for 5 and 20 mm gaps in Fig. 5, are in agreement with the model in Eqn. 5, which has been plotted on top of the noise spectrum data using the values of  $\Delta S_{F_0}$  and  $\tau$

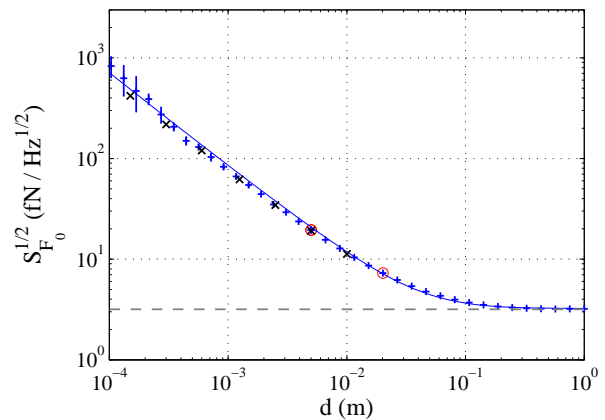


FIG. 3: Simulation data (blue dots) for the force noise linear spectral density as a function of the gap,  $d$ , for  $p = 2 \times 10^{-6}$  Pa, with a fit to the simple analytical model (Eqn. 20). The dashed gray line is the theoretical infinite gap limit. Points at  $d$  of 5 and 20 mm are circled to indicate, respectively, the geometries of the baseline and alternative designs discussed in the conclusion. Points shown as black “x” are simulation data for the molecular escape time, converted into force noise using the model in Sec. III A.

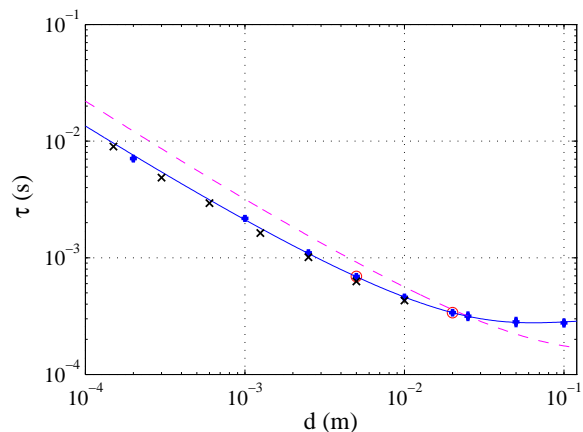


FIG. 4: Value of the characteristic time constant  $\tau$  extracted from the simulation force fluctuations (blue dots), as a function of gap  $d$ , using the model in Eqn. 6. The dashed pink curve represents the raw result of the approximate analytic model (Eqn. 14) in Sec. III B, while the solid blue curve represents a two parameter fit to the same model, discussed in the text. Again, circled points at 5 and 20 mm indicate the baseline and alternate geometries. Points marked with a black “x” are simulation values for the average molecular escape time from the intercylinder gap, which correspond approximately to the values of  $\tau$  extracted from the force fluctuations.

obtained from  $\langle(\Delta q)^2\rangle$  as described above and presented in Figs. 2 - 4.

A variation on this simulation can be used to extract the average escape time for a molecule inside the intercylinder gap. Here, the initial position of the molecule is distributed uniformly inside the cylindrical space be-

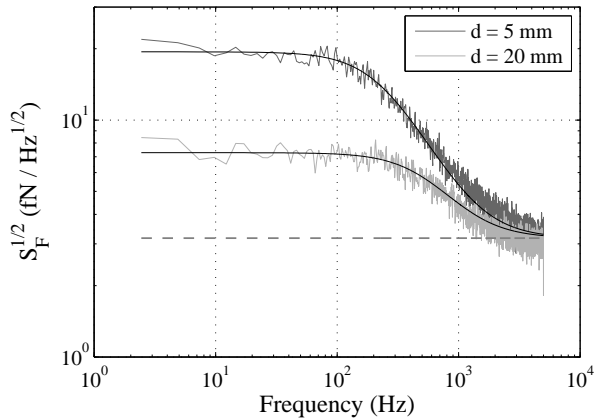


FIG. 5: Simulation force noise linear spectral density as a function of frequency for 5 and 20 mm gaps, using  $p = 2 \times 10^{-6}$  Pa. Also plotted, with solid black lines, is the model from Eqn. 5, using the parameters extracted from the data in Fig. 2. The dashed gray line corresponds to the force noise in the infinite volume limit.

tween TM and RM, with the simulation run until the molecule exits this gap. This has been performed for 7 values of  $d$ , each time averaging over 10000 trial molecules. These data are plotted with the values of  $\tau$  extracted from the force fluctuations in Fig. 4. The agreement, at the 10-15% level, with the time constant relevant to the force noise spectrum rolloff, confirms the intuitive interpretation of diffusion time discussed in the introduction. Additionally, as will be discussed in the following section, the diffusion time  $\tau(d)$  is linked directly, with a simplified analytical model, to an estimate of the resulting force noise. This projection for the white noise level is shown here in Fig. 3.

Before discussing the quantitative impact of the observed noise increase on the gravitational wave detection sensitivity, we turn first to a discussion of the physics of excess gas damping in the context of simplified analytical models and then to the experimental evidence underpinning the simulation and predictions.

### III. COMPARISON WITH SIMPLIFIED ANALYTICAL MODELS

A combination of simple analytical models is useful for illuminating the physics of proximity-enhanced gas damping, but also for arriving at a closed form approximate expression for the excess force noise as a function of the gap  $d$ .

#### A. Macroscopic damping for a piston weakly connected to an external gas reservoir

A simple macroscopic model for proximity-enhanced gas damping, following the discussion in the introduction

and Refs. [6, 8], comes from approximating the inter-cylinder gap as an isothermal volume at uniform pressure connected to the external gas reservoir at pressure  $p$  via a molecular flow impedance,  $Z_M$ , with units of  $[s/m^3]$ . In the presence of a displacement  $x(t)$  of the TM along its symmetry axis, the volume is  $V = \pi R^2(d+x)$ , and we can express the pressure as  $p + \delta p(t)$ . We can then write the standard ideal gas and molecular flow equations for the instantaneous number of molecules  $N_0$  in the gap,

$$\begin{aligned} k_B T N_0 &= (p + \delta p) \pi R^2 (d + x) \\ k_B T \frac{dN_0}{dt} &= -\frac{\delta p}{Z_M} \end{aligned} \quad (8)$$

Considering small displacements  $x \ll d$ , these expressions can be combined into a linearized equation for  $\delta p$ ,

$$\frac{d\delta p}{dt} + \frac{\delta p}{\tau} = -\frac{p}{d} \frac{dx}{dt}, \quad (9)$$

where we have reexpressed the molecular impedance in terms of the effective pressure equilibration time  $\tau = Z_M V = Z_M \pi R^2 d$ , analogous to an  $RC$  discharge time.

To calculate the mechanical impedance, or relationship of force to velocity  $v$ , Eqn. 9 can be evaluated in the frequency domain for harmonic TM motion, using  $v = i\omega x$ . The pressure increase  $\delta p$  is multiplied by surface area to obtain force,

$$F = -\pi R^2 \frac{p\tau}{d} \frac{i\omega x}{1 + i\omega\tau} = -v \times \pi R^2 \frac{p\tau}{d} \frac{1 - i\omega\tau}{1 + (\omega\tau)^2}. \quad (10)$$

Equation 10 describes a mechanical impedance that is primarily real and thus dissipative at lower frequencies. At higher frequencies, the impedance becomes imaginary, and thus a lossless spring as gas compression occurs without sufficient time for gas flow out of the gap. For the force noise, the fluctuations-dissipation relation in Eqn. 1 can be evaluated with the real part of Eqn. 10 to yield

$$\Delta S_F = 4k_B T \times \pi R^2 \frac{p\tau}{d} \frac{1}{1 + (\omega\tau)^2}. \quad (11)$$

This low-pass form of the predicted force noise is indeed confirmed by the simulations, in Figs. 2 and 5.

For the interaction-free regime studied here, the pressure equilibration time  $\tau$  is equivalent to the average time that a molecule needs to escape from the gap into the surrounding gas reservoir. This escape time is plotted in Fig. 4 and, converted into a low frequency force noise level using Eqn. 11, Fig. 3. This macroscopic picture is approximate in that it assumes the pressure inside the gap to be uniform, while physically there must be a radial pressure gradient in order to drive gas flow out of the gap upon squeezing. Nonetheless, there is a remarkable agreement for the cylindrical geometry between the average escape time and the simulation force fluctuation values for force noise and time constant  $\tau$ .

To complete a predictive analytical model for proximity damping, we require an independent estimate for the time constant  $\tau(d)$ , which contains the physics of the molecular diffusion process and is addressed in the following subsection.

## B. Random walk calculation of escape time $\tau$

The escape time  $\tau$  can be estimated by simple random walk arguments for a molecule in the intercylinder gap. This model is relevant in the limit  $d \ll R$ , with a typical molecule making many collisions before escaping the gap.

The number of collisions  $N$  that a particle makes before diffusing out of the intercylinder gap can be estimated from the random walk mean square distance traveled along a direction perpendicular to the cylinder axis, or  $N\langle r^2 \rangle$ , where  $\langle r^2 \rangle$  is the mean square lateral displacement that a particle makes in a single flight between opposing faces of the two cylinders. Thus, covering a distance  $R$  to diffuse out of the gap will require  $N \approx \frac{R^2}{\langle r^2 \rangle}$ . The characteristic time  $\tau$  that a molecule takes to random walk out of the gap will thus be  $\tau \approx N\langle t \rangle$ , where  $\langle t \rangle$  is the average time of flight to cross the gap between opposing faces of the two cylinders.

Estimates of  $\langle r^2 \rangle$  and  $\langle t \rangle$  can be calculated analytically for a particle emitted, with cosine-law distribution, from the center of one of the cylinder faces into the gap of height  $d$  and radius  $R$  (see Appendix C):

$$\begin{aligned} \langle r^2 \rangle &\approx d^2 \ln \left[ 1 + \left( \frac{R}{d} \right)^2 \right] \\ \langle t \rangle &\approx \left( \frac{\pi}{2} \right)^{1/2} \frac{d}{v_T} . \end{aligned} \quad (12)$$

We can use these values to estimate  $N$ ,

$$N \approx \frac{R^2}{\langle r^2 \rangle} \approx \frac{R^2}{d^2 \ln \left[ 1 + \left( \frac{R}{d} \right)^2 \right]} \quad (13)$$

and then the molecular escape time  $\tau$ ,

$$\tau \approx N\langle t \rangle \approx \left( \frac{\pi}{2} \right)^{1/2} \frac{R^2}{dv_T \ln \left[ 1 + \left( \frac{R}{d} \right)^2 \right]} . \quad (14)$$

Inserting the result of Eqn. 14 into Eqn. 11 and recalling the thermal velocity  $v_T \equiv \sqrt{k_B T/m}$ , we obtain the low frequency force noise

$$\Delta S_{F_0} \approx p(8\pi m_0 k_B T)^{1/2} \pi R^2 \frac{R^2}{d^2 \ln \left[ 1 + \left( \frac{R}{d} \right)^2 \right]} . \quad (15)$$

The force noise thus has a prefactor – proportional to  $p$  and surface area  $\pi R^2$  – similar to the infinite volume result (Eqn. 3), multiplied by a dimensionless excess factor that depends on the aspect ratio via  $R/d$ .

This model for  $\tau$  and  $S_{F_0}$  is also approximate. The true mean square displacement  $\langle r^2 \rangle$  depends on the position on the cylinder face from which the particle is emitted, as will the expected full escape time. Additionally, the model treats the random walk as a Gaussian process, with the mean square step size as the single parameter

characterizing the statistics. For  $R/d \rightarrow \infty$  this approximation is catastrophic, as the variance of the step diverges (see App. C and Ref. [6]). However, for the scope of estimating the diffusion time out of a finite radius cylindrical volume, the calculation of the step size variance can be truncated to consider steps no larger than  $R$ . As seen in earlier studies[5] and as will be shown in the next sections, this is a good approximation to the physics seen in the simulations.

## C. Equivalent shot noise model

Independently from the macroscopic piston damping model in Sec. III A, the calculation of  $\tau$  in Sec. III B can be used for direct estimate of the force noise using a shot noise model. Here, the “shot” of momentum corresponds not to the momentum exchange of a single molecular impact, but rather to the total momentum exchanged by a single molecule over  $N$  impacts with the TM before escaping from the intercylinder gap.

The force shot noise can be expressed

$$\Delta S_{F_0} = 2(\delta q)^2 \lambda \quad (16)$$

The characteristic impulse  $\delta q$  is the typical thermal momentum exchange of a single collision ( $2m_0 v_T$ ) multiplied by the number  $N$  of collisions that a molecule makes with the TM on a typical pass through the the gap,

$$\delta q \approx 2N m_0 v_T . \quad (17)$$

The characteristic rate of such summed impulses,  $\lambda$ , is the rate at which molecules enter, and exit, the intercylinder gap. This is the expected number of molecules between the cylinders divided by the diffusion time  $\tau$ ,

$$\lambda \approx \frac{p}{k_B T} \times \pi R^2 d \times \frac{1}{\tau} \quad (18)$$

Finally, insertion of these values into Eqn. 16 gives the force shot noise,

$$\begin{aligned} \Delta S_{F_0} &\approx 2(4N^2 m_0 k_B T) \times \left( \frac{p}{k_B T} \pi R^2 d \frac{1}{\tau} \right) \\ &\approx \frac{4}{\pi} p (8\pi m_0 k_B T)^{1/2} \pi R^2 \frac{R^2}{d^2 \ln \left[ 1 + \left( \frac{R}{d} \right)^2 \right]} \end{aligned} \quad (19)$$

This shot noise prediction differs from that of Eqn. 15 by the numerical factor  $\frac{4}{\pi}$  and thus, at the approximate level of this calculation, can be considered equivalent to Eqn. 15.

## D. Comparison with simulation results

Using Eqn. 15 as a model for the excess gas damping force noise, a fit of the simulation data for  $S_{F_0}$  to the

model

$$S_{F_0}(d) \approx AS_F^\infty + Bp(8\pi m_0 k_B T)^{1/2} \pi R^2 \left\{ \frac{R^2}{d^2 \ln \left[ 1 + \left( \frac{R}{d} \right)^2 \right]} - 1 \right\} \quad (20)$$

is shown in Fig. 3. Here,  $S_F^\infty$  is defined as in Eqn. 3, and the subtraction of unity in the second term is inserted to give a null contribution for  $d \rightarrow +\infty$ , attributing all residual damping to the infinite volume term. We obtain  $A = 1.038 \pm 0.004$  and  $B = 0.78 \pm 0.005$ . The value of the excess damping factor  $B$  is of order unity, indicating that this simplified model indeed gives the right magnitude of the excess damping, though the observed agreement at the 25% level is perhaps better than expected given the approximations of the model. It is likely that the finite size of the simulated system is responsible for the several percent excess observed for the infinite gap limit (coefficient  $A$ ).

While the fit of this approximate model is not particularly good by statistical standards, with  $\chi^2 \approx 12$ , this model nonetheless gives a useful analytical formula for  $S_F$  as a function of gap, with 30% accuracy in noise power spectral density across four decades of  $d$ . We note that fitting to a model that neglects the logarithmic contribution – thus considering the excess damping term as  $\Delta S_{F_0} \propto d^{-2}$  – deviates from the simulation data by more than a factor 2 across the same range. Similarly unsatisfactory results are obtained with other power law fits, which can work well over a given single decade in  $d$  but not wider ranges, with the logarithmic slope observed to change, steepening towards -2 with decreasing gap. This confirms the basic physics given in Sec. III B.

The values of  $\tau$  extracted from Eqn. 6 are shown in Fig. 4. These are compared with values associated with the simulation mean escape time from the gap. Shown as a dashed curve is a simple, unscaled plot of the approximate analytical estimate of  $\tau$  from Eqn. 14 [29], which is within a factor 2 of the simulation results across the three decades of  $d$  for which we extract  $\tau$ . Also shown, with a solid curve, is a two parameter fit to the data, using Eqn. 14 but allowing multiplicative prefactors both to the overall expression for  $\tau$  and as a scale factor for  $d$  in the logarithmic term. This gives a statistically good fit, with the relevant scale factor effectively lengthening  $d$  in the logarithmic term, by 3.2 (equivalently, shortening  $R$ ). This is likely related to the oversimplification of assuming molecules starting from the geometric center – and not a range of positions in the intercylinder gap – in our calculations of  $N$ ,  $\langle t \rangle$ , and  $\langle r^2 \rangle$ . We note that similar scaling of  $d$  in the logarithmic term for the force noise  $S_{F_0}$ , discussed in the preceding paragraph, has no relevant impact on the quality of the fit in Fig. 3.

#### IV. SUMMARY OF EXPERIMENTAL EVIDENCE

Two recent experimental efforts provide a verification of the general physics of proximity-enhanced gas damping and of the simulation techniques employed in this study. Aside from the specifics of the geometries studied, the simulations used to analyze these experiments differ from those described in Sec. II only in that they estimate a rotational damping coefficient,  $\beta_{rot} = \frac{S_N}{4k_B T}$ , using the fluctuations in the average torque, rather than force. Both experimental studies calculate the gas contribution to  $\beta_{rot}$  from measured torsion pendulum free-oscillation decay, characterized by energy decay time constant  $\tau_e$  or, equivalently, the quality factor  $Q$ ,

$$\frac{1}{\tau_e} = \frac{2\pi f_0}{Q} = \frac{\beta_{rot}}{I}, \quad (21)$$

where  $f_0$  is the pendulum resonant frequency and  $I$  is its moment of inertia.

Figure 6 displays the data for the measured rotational gas damping coefficient  $\beta_{rot}$  from the University of Trento (UTN) torsion pendulum ringdown measurements[5] with two pendulum geometries featuring cubic TM (46 mm side). Proximity-enhanced gas damping is studied in the geometry relevant to the LISA gravitational wave observatory, where the TM is enclosed by a rectangular capacitive sensor electrode housing – referred to here as gravitational reference sensor (GRS) – with 3-4 mm gaps[5]. In the first configuration (1TM), the cubic TM is suspended on axis and thus a pure rotational damping is measured. In the second configuration (4TM), four TM are each displaced by roughly 11 cm from the pendulum rotation axis in a cross configuration. This results in both translational and rotational damping inside electrode housings that surround two of the TM (one housing is the GRS mentioned above and the other is a larger housing with 6-8 mm gaps). Measurements with the 4TM were also performed after removing the GRS housing (labeled “w/o GRS” in the plot), in order to isolate its proximity effect on the total damping. From each dataset the zero-pressure background pendulum damping has been subtracted off using a linear fit. This is nearly irrelevant for the 1TM data, which employs a low damping fused silica fiber[14] –  $Q \approx 10^6$  – while for the 4TM experiment, using tungsten fibers with  $Q \approx 2000 - 3000$ , the fiber damping is ten times larger than the gas damping contribution at the lower pressures of the study. Here, uncertainty in the residual damping is the dominant source of error and causes the large spread in the data (several points with error bars overlapping zero have been omitted from the log-scale plot, but have been used in obtaining the fits to the 4TM data).

The UTN data demonstrate the proportionality of gas damping to pressure, for more than three decades in pressure in the 1TM study and more than a decade in pressure in the 4TM study, with the wide dispersion mentioned above limiting the validity at lower pressures. All



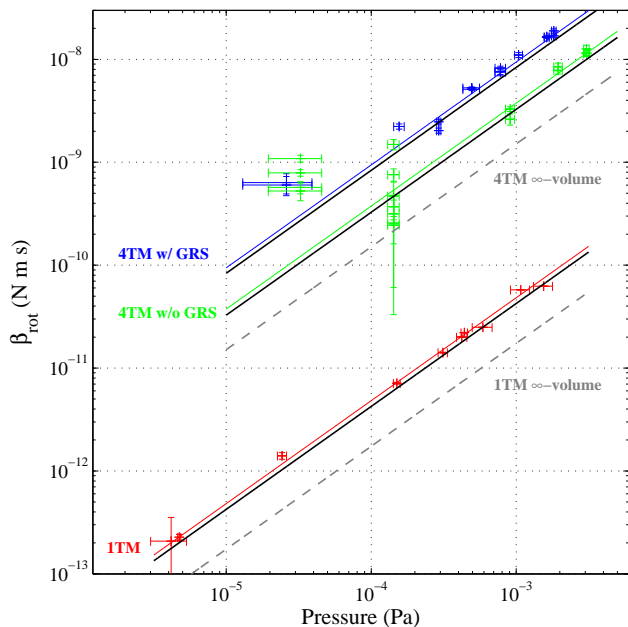


FIG. 6: Plot of experimental data from the UTN gas damping experiment [5] featuring cubic test masses in two different torsion pendulums dominated by rotational (1TM) and translational (4TM) squeezing, the latter with two different conditions of proximity to the surrounding apparatus. The pressure independent damping has been removed from each dataset to show only the gas contribution. Linear fits to each dataset are shown. The simulation predictions for the three cases are shown as thick black lines, while the infinite volume limit predictions for the two pendulums are shown in dashed gray.

the data demonstrate a clear – factor 3 to 6 – excess above the predictions of the infinite volume model calculated from Ref.[4]. Additionally, the measurable decrease in gas damping for the identical pendulum upon removal of the GRS in the 4TM pendulum can only be attributed to proximity damping. The three datasets are consistent, at the 20% level, with simulations that employ the same technique as that described for the LIGO configuration in Sec. II, with the torque damping coefficient calculated from the simulation torque fluctuations. Though based on the same basic cubic geometry and gap sizes, the different measurements probe both the translational and rotational aspects of squeezing, which have slightly different dependence on gap.

Not shown here, the UTN experiments [5] also verified the Brownian nature of the force fluctuations associated with the gas damping, detecting a frequency independent increase in the pendulum torque noise floor consistent with  $S_N = 4k_B T \beta_{rot}$ .

The University of Washington (UW) experiments [6], with results shown in Fig. 7, measure the gas pressure ringdown damping of a two different torsion pendulums. Both inertial members, labeled NTA and LTA, are thin rectangular plates in close proximity to a second parallel plate, with the NTA dimensions 42 mm  $\times$  31 mm  $\times$  2 mm

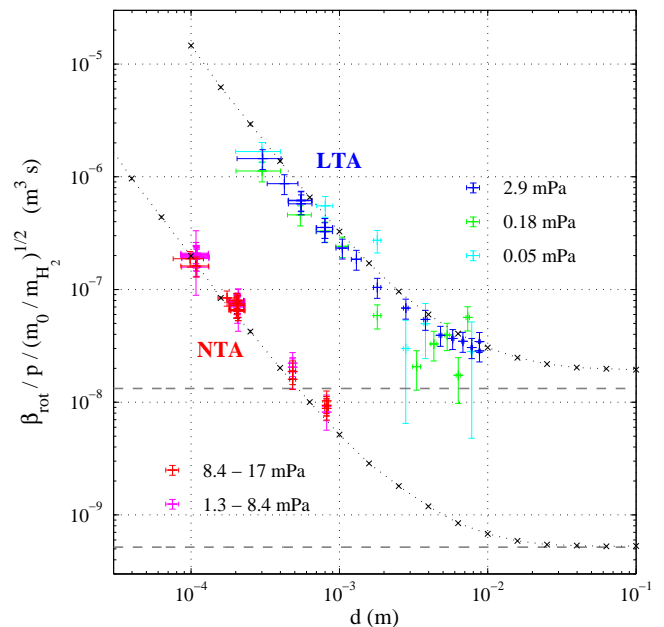


FIG. 7: Plot of experimental data from the UW gas damping experiment [6] for two different torsion pendulums, labeled NTA and LTA, both with a rectangular plate geometry in proximity of a second parallel plate at distance  $d$ . The pressure independent damping has been removed from each dataset to show only the gas contribution. Simulation points are shown with black  $\times$ , with infinite volume limits shown in dashed gray. Dotted lines connecting simulation points are included as a guide for the eye.

and the LTA dimensions 114 mm  $\times$  38 mm  $\times$  450  $\mu$ m. Separations from 100  $\mu$ m to 1 cm are studied, covering a range of aspect ratios –  $b/d$ , with  $b$  the shorter dimension of the rectangular plate – of 4 to 400, thus well bracketing the LIGO geometry, where  $2R/d \approx 70$ . The data have been normalized for linear pressure dependence, as well as for the different atomic masses of the residual gas species, mostly  $N_2$  and  $H_2O$ , using  $\beta \sim p m_0^{1/2}$ . For each dataset the pressure independent damping has been estimated, and removed, using the zero-pressure intercepts from linear fits to groups of damping measurements performed at fixed gap  $d$ .

In addition to distributing statistically around a single curve following normalization for pressure, the data demonstrate the increase in damping with decreasing gap, by roughly two orders of magnitude for a factor 30 decrease in gap for the LTA data. Also shown with the data in Fig. 7 are the predictions from the torque noise simulation performed for this geometry as in Sec. II. The simulation  $\beta_{rot}$  agrees with the experimental data to within 30% across two decades of  $d$ , with residual differences considered compatible with systematic and statistical uncertainties in assigning pressures and gas species.

Even for the largest gaps studied,  $b/d \approx 4$  for LTA, excess proximity damping is dominant over the infinite volume contribution. The simulation for large  $d$  is com-



plicated by the presence of additional fixed control surfaces, adding proximity damping that is independent of  $d$ [15]. As seen in Fig. 7, inclusion of geometrically simple control electrode surfaces in the LTA simulation create a relevant increase of the large  $d$  predictions above the infinite volume prediction [30]. Thus, while the experimental data are consistent with the simulation at total damping values only several times larger than the infinite volume limit, they do not allow a quantitative comparison with the infinite volume predictions.

The UW results are incompatible with an elastic, specular scattering description of the molecule - wall interaction. With elastic scattering, the molecule velocity parallel to the plate surfaces is unchanged as it bounces through the gap, and so the effective escape time  $\tau$  becomes independent of gap. Following Eqn. 11, this would give force noise  $S \sim \beta \sim d^{-1}$ . The steeper gap dependence observed in Fig. 7, with logarithmic slopes of approximately  $-1.5$  in the decade of smallest gap in both configurations, is thus incompatible with an elastic scattering scenario. Along with the success of the simulations in explaining the data, at least for the systems under study here – involving gold coated surfaces and mostly water vapor and nitrogen residual gas at room temperature – the diffuse inelastic scattering hypothesis is well verified.

Taken as a whole, the two experimental campaigns measure proximity-enhanced gas damping at levels that agree with simulation predictions to better than 30% over several orders of magnitude in both pressure and gap size. Such a quantitative test of the physics and simulation techniques employed here for Advanced LIGO, in similar macroscopic systems, strengthens the confidence in the predictions for the gravitational wave sensitivity, which are discussed in the next section.

## V. IMPACT ON GRAVITATIONAL WAVE DETECTION CAPABILITIES AND DISCUSSION

The data for  $S_{F_0}$  and  $\tau$  with  $d = 5$  mm, in Figs. 3 and 4 correspond to the current Advanced LIGO design geometry. The low frequency noise power increase (or equivalently, the increase in the gas damping coefficient  $\beta$ ), with respect to the infinite volume limit is near 40, or slightly more than 6 in linear force noise spectral density.

Considering a design gas pressure of  $2 \times 10^{-6}$  Pa ( $1.5 \times 10^{-8}$  Torr) of  $H_2$ , this contributes a white low frequency force noise  $S_{F_0}^{1/2} \approx 20$  fN/Hz $^{1/2}$ , or an acceleration noise of nearly  $0.5$  fm/s $^2$ /Hz $^{1/2}$ . This acceleration noise is assumed to act equally on each of the four TM in the two interferometry arms. Converted into an equivalent gravitational wave strain noise with 4 km interferometry arms, the white force noise assumes an approximate  $f^{-2}$  shape in  $S_h^{1/2}$  at low frequencies, and, as shown in Fig. 8, rivals quantum fluctuations as the leading noise source in the 10 - 30 Hz band [16][31]. This can have a significant im-

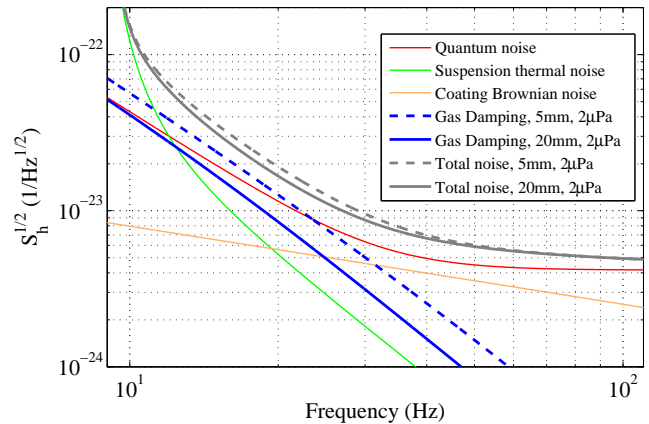


FIG. 8: Gravitational wave strain measurement noise contributions for Advanced LIGO[16]. Dashed and solid blue curves correspond to the noise contributions from gas damping noise with  $2 \times 10^{-6}$  Pa of  $H_2$  for the nominal geometry (all 5 mm gaps between all four TM - reaction masses pairs) and the alternate geometry with a 20 mm gap adjacent to the two input TM. The total measurement noise in the two geometries are shown with thick gray curves.

part on the detection horizon for observing neutron star inspirals, even more so for the merger of more massive black hole sources, which have more signal contribution at the lowest frequencies.

We note that the calculated diffusion time is fast enough,  $700 \mu\text{s}$ , that the corresponding 3 dB rolloff frequency of roughly 230 Hz is above the band where gas damping is critical to the detector sensitivity, with photon shot noise limiting sensitivity at these frequencies for the advanced detectors.

The non-trivial impact of this noise source on the Advanced LIGO sensitivity has raised the attention of the collaboration[17], and we consider here a few options for mitigation. For the central input TM (ITM), increasing the gap between ITM and the reaction mass to 20 mm is feasible, which reduces the associated force noise power on the ITM by roughly a factor 7 (see Figs. 3 and 5). The ITM reaction masses, called compensation plates, are used for correcting the beam wavefront for thermal lens effects and for relatively low force authority electrostatic actuators. The reaction masses associated with the distant end TM (ETM), on the other hand, are responsible for higher authority electrostatic force control of the interferometer cavity length, and increasing the gap would create a serious limit on the maximum possible force. As such, the current baseline design maintains 5 mm gaps for the ETM. Mitigation for the ETM force noise could be achieved by improving the vacuum pressure at the end stations or, if necessary, adopting a more complicated, possibly ring-like, geometry for the electrostatic actuation reaction masses. The gas damping and total gravitational wave strain with the increased ITM gaps is also shown in Fig. 8.

It is worth reconsidering one initial assumption used

in this analysis, namely that the steady state pressure in the gap is equal to that of the surrounding gas reservoir. In practice, any local outgassing from the surfaces inside the gap will create a net radial molecular flux and thus a local pressure increase above that of the surroundings. This increased effective pressure in the gap increases the corresponding force noise, and thus maintaining the predictions obtained for  $2 \mu\text{Pa}$  of  $\text{H}_2$  limits the tolerable outgassing from the test and reaction mass surfaces. The pressure increase from a total gas outgassing flux  $Q$  (measured in  $[\text{Pa m}^3/\text{s}]$ ) can be estimated from the macroscopic flow estimates of Sec. III A,

$$\Delta p = Q Z_M = Q \frac{\tau}{\pi R^2 d} . \quad (22)$$

Given the estimated values of  $\tau$  in Sec. II, maintaining  $\Delta p$  well below  $2 \mu\text{Pa}$  in the 5 mm gap will require outgassing well below  $10^{-6} \text{ Pa m}^3/\text{s}$ . Per surface area, this corresponds to  $10^{-8} \text{ mBar l/s/cm}^2$ , using more familiar vacuum technology units. This represents an important – but, with reasonable pumping times and temperatures, feasible – requirement on outgassing performance, which is likely to be dominated by water outgassing from the optical surfaces[18, 19].

In closing, we discuss a series of design concerns relevant to other observatories with goals similar to those of Advanced LIGO, such as Advanced Virgo[20] and the Large-scale Cryogenic Gravitational wave Telescope (LCGT [21, 22]), and to more ambitious future facilities, such as the Einstein Telescope (ET [23]). The first issue is geometrical. Instead of simply increasing the distance between similar shaped test and reaction masses as in Advanced LIGO, which improves the linear noise spectral density roughly proportionally to  $d$ , the proximity enhancement can be effectively removed for a reaction mass in the form of an external coaxial ring around the cylindrical TM. In this geometry, TM motion along the cylinder (and GW-measurement) axis does not compress the gas between the TM and reaction ring. As such there is no gas flow in the gap and no related excess proximity dissipation. The same physics explains the absence of excess force noise perpendicular to the cylinder axis in the Advanced LIGO geometry seen in Sec. II.

Advanced Virgo employs such an external ringlike reaction mass. There is an additional cylindrical thermal compensation plate facing the TM cylinder, but at a distance of 20 cm [20] and thus virtually irrelevant for its proximity (see Fig. 3). Considering the vacuum requirements, dominated by  $10^{-7} \text{ Pa}$  of  $\text{H}_2\text{O}$ , and TM dimensions similar to those of Advanced LIGO, one expects a number several times below that given in Eqn. 3, and thus not a critical issue for the target sensitivity.

Proximity concerns aside, gas damping can be reduced by acting on the factors relevant to the infinite volume limit, concerning the TM thermal vacuum environment, which enter as a factor  $p^{1/2} T^{1/4} m_0^{1/4}$  in linear spectral density, and the TM geometry, entering roughly as the ratio of the square root of the the surface area ( $R$ ) to mass

( $R^2 h$ ). LCGT will employ cryogenically cooled TM, at 20 K, with expected pressures near  $2 \times 10^{-7} \text{ Pa}$  dominated by  $\text{H}_2$ . LCGT will thus enjoy a rough factor 6 noise improvement over Advanced LIGO before considering geometry (LCGT will also likely employ a ring geometry for the reaction masses[24]). Though the TM are slightly smaller than those of Advanced LIGO (30 kg of sapphire rather than 40 kg of fused silica), there should be a net improvement with LCGT and thus gas damping should not be critical for their design sensitivity.

Several cryogenic issues complicate the gas damping analysis. The molecules striking the TM are assumed to have been thermalized by a cryogenic thermal shield, but some alteration of the velocity distribution by thermal gradients is still possible. Low temperatures should enable lower pressure with cryopumping, freezing out all relevant species except  $\text{H}_2$ . More delicate, but potentially helpful, is the question of  $\text{H}_2$  sticking on the TM. Sticking times for  $\text{H}_2$  on cold solid surfaces rapidly lengthen with decreasing temperature, with a strong substrate dependence, from the  $\mu\text{s}$  - ms range at 20 K to the 1 s - 1 year range at 10 K (see App. A). While we do not have published absorption parameters for  $\text{H}_2$  on the most probable oxide TM coatings, such as  $\text{SiO}_2$  and  $\text{Ta}_2\text{O}_5$ , it is likely that sticking times can rival or exceed time-of-flight to surrounding surfaces (of order  $20 \mu\text{s}$  for 5 mm at 20 K). This lengthens the relevant escape time  $\tau$  and progressively lowers the maximum frequency for which proximity effects are relevant, even to below the band of interest[32].

The Einstein Telescope, which has a dedicated low frequency interferometer, aims at sensitivities of roughly  $10^{-24}/\text{Hz}^{1/2}$  at 10 Hz with an increased armlength of 10 km and thus requires a factor 30 improvement over the Advanced LIGO acceleration noise. This will require both an improved geometrical configuration, such as the just discussed ring reaction mass design, and some combination of improved thermal vacuum conditions and larger TM. The specified conditions ( $10^{-8} \text{ Pa}$  and 10 K) alone give a factor 30 improvement over the same values for Advanced LIGO. TM of roughly 200 kg and 500 mm diameter will give an extra factor 3 improvement for the infinite volume prefactor. Assuming that the target pressure is reached, gas damping does not appear to be a dominant noise source for ET.

## Appendix A: Estimation of molecular sticking time

The sticking time, which we will call  $\tau_{st}$ , or average time that a molecule spends on the surface of the test mass or adjacent apparatus between impact and reemission, can be evaluated via its influence on the two dimensional equation of state of the adsorbed film in equilibrium with its gas vapor. This is characterized by number density  $n_{2D}(p, T)$ . In equilibrium, the rate of molecules (per area) that desorb from the surface to enter the gas phase,  $\frac{n_{2D}}{\tau_{st}}$ , must be equal to the number of gas molecules

that strike the surface[25]. Integration over the Maxwell-Boltzmann velocity distribution gives the latter, and we find[33]

$$\frac{p}{(2\pi m_0 k_B T)^{1/2}} = \frac{n_{2D}}{\tau_{st}}. \quad (\text{A1})$$

For the low gas pressures and relatively high temperatures of interest to our experimental system, we consider the adsorbed molecules as an ideal non-interacting 2D gas in the  $xy$  plane, with a substrate potential  $V(z)$  in the dimension perpendicular to the surface. Approximating the surface potential with a well depth  $D$  and elastic constant  $m_0\omega^2$ , this gives energy levels

$$\epsilon = \frac{\hbar^2 k^2}{2m_0} - D + \hbar\omega \left( n + \frac{1}{2} \right)$$

where  $k$  represents the 2D wave vector. In the classical limit of low occupation number, this yields the following equation of state

$$n_{2D} = \frac{p}{k_B T} \left( \frac{2\pi\hbar^2}{m_0 k_B T} \right)^{1/2} \exp \frac{D}{k_B T} \frac{1}{2 \sinh \frac{\hbar\omega}{2k_B T}}. \quad (\text{A2})$$

Combining this with Eqn. A1, we obtain

$$\tau_{st} = \frac{2\pi\hbar}{k_B T} \exp \frac{D}{k_B T} \frac{1}{2 \sinh \frac{\hbar\omega}{2k_B T}}. \quad (\text{A3})$$

An intuitive, semi-classical interpretation of this sticking time emerges in the limit of classically excited oscillator states, with  $\hbar\omega \ll k_B T$ , which yields

$$\tau_{st} \approx \frac{2\pi}{\omega} \exp \frac{D}{k_B T}. \quad (\text{A4})$$

This limit corresponds to a molecule oscillating around the bottom of the potential well, ‘‘attempting escape’’ once per classical oscillation, with an Arrhenius escape probability of  $\exp \frac{-D}{k_B T}$ .

Substituting a harmonic well for the true Van der Waals potential with Coulomb repulsion is an approximation, both for the level spacing and for the finite number of bound states. Additionally, this model treats possible rotational excitations of the molecule as equally populated in the gas and adsorbed phases. As such, we use this model only to have an order of magnitude estimate of sticking times, to give a comparison with the typical times of flight between collisions on adjacent test mass and reaction mass surfaces.

Typical measured values for the adsorption well depth of  $\text{H}_2$  on various solid substrates, including both dielectrics and metals, range from 300 to 600 K, with oscillator level spacings of order several hundred K [26]. This results in room temperature sticking times of order 1 ps. The distinction between the classical and quantum excitation levels of harmonic oscillator is a minor correction to the sticking time estimates here, and the sticking

times correspond to several to tens of classical oscillation cycles. More easily polarized molecules such as  $\text{N}_2$ ,  $\text{CH}_4$ , and  $\text{H}_2\text{O}$  can find adsorption well depths of order 1000 K with slightly lower vibrational energies, resulting in sticking times of order 10-100 ps. For all realistic residual gas species, the room temperature sticking times are sub-ns, well below the typical times for a gas molecule to cross a 5 mm gap, which is of order 5  $\mu\text{s}$  for  $\text{H}_2$  and longer for larger molecules. As such, the sticking time of residual gas molecules in Advanced LIGO is not expected to create a relevant departure from the time dependence of force fluctuations given using the approximation of immediate reemission of incoming gas molecules.

For cryogenic temperatures, such as the 20 K foreseen for LCGT, the situation is quite different. Bound molecules are frozen into the ground state of the adsorption potential well, with a binding energy  $(D - \frac{\hbar\omega}{2})$ . The sticking time for  $\text{H}_2$  on the dielectric surface of foreseen oxide coatings such as  $\text{SiO}_2$  or  $\text{Ta}_2\text{O}_5$  becomes very sensitive to the adsorption parameters – for which we do not have published values – and the exact temperature. For instance, for  $\text{H}_2$  on the oxide  $\text{MgO}$ , with binding energy 330 K, the estimated sticking time is of order 0.5 ms, with a 10% change in either binding energy or temperature producing a factor 5 change in the sticking time. For  $\text{H}_2$  on  $\text{NaCl}$  (280 K binding energy) and on graphite (440 K), the sticking times are 3  $\mu\text{s}$  and 7 ms. At 10 K, the range of  $\tau_{st}$  for these species becomes 10 s to 1 year.

In the Advanced LIGO-like geometry at cryogenic temperatures, it is thus conceivable that the sticking time will be longer than the time for molecules to cross the intercylinder gap. Though this complicates the analysis, the general effect on gas damping can be understood with the force shot noise model discussed in Sec. III C. At a given  $p$  and  $T$ , sticking will not change the total momentum exchange associated with a molecule’s stay inside the gap or the rate at which molecules enter the gap, but it will lengthen the typical time spent inside the gap by  $N \tau_{st}$  ( $N$  is the typical number of collisions that a molecule makes before diffusion out of the gap, Sec. III, of order 100 for 5 mm gaps in Advanced LIGO). As such, the low frequency force noise should be unchanged by sticking, but the longer diffusion or correlation time results in a lower frequency cutoff for the excess noise from any proximity effects. This could push any excess proximity damping to frequencies below the band of interest.

## Appendix B: Calculation of $\langle \Delta q^2 \rangle$

For a zero mean, statistically stationary random variable  $F(t)$  with mean defined over some time interval  $[0, T_0]$ ,  $\bar{F} \equiv \frac{1}{T_0} \int_0^{T_0} F(t) dt$ , the expected fluctuations in  $\bar{F}$  can be calculated in terms of the autocorrelation func-

tion  $C_{FF}(\delta) \equiv \langle F(t) F(t + \delta) \rangle$ ,

$$\langle \bar{F}^2 \rangle = \frac{1}{T_0} \int_{-T_0}^{T_0} C_{FF}(\delta) \left(1 - \frac{|\delta|}{T_0}\right) d\delta. \quad (\text{B1})$$

In our case,  $F(t)$  is the instantaneous force felt by the TM due to molecular impacts.

The single-sided power spectrum  $S_F(\omega)$  is defined by the Fourier transform of  $C_{FF}(\delta)$ ,  $S_F(\omega) = 2 \int_0^\infty C_{FF}(\delta) \exp(-i\omega\delta) d\delta$ . For a process characterized by white noise passed through an effective low-pass filter, such as our approximation of the gas damping system studied here, with  $S_F = \frac{S_0}{1+(\omega\tau)^2}$ , the corresponding autocorrelation function can be calculated to be

$$C_{FF}(\delta) = \frac{S_0}{4\tau} \exp\left(-\frac{|\delta|}{\tau}\right). \quad (\text{B2})$$

Inserting this result into Eqn. B1 and integrating, we obtain

$$\langle \bar{F}^2 \rangle = \frac{S_0}{2T_0} \left[1 - \frac{1 - \exp\left(-\frac{T_0}{\tau}\right)}{\frac{T_0}{\tau}}\right]. \quad (\text{B3})$$

As the total momentum exchange with the TM in a measurement time  $T_0$  is simply  $\Delta q = \bar{F}T_0$ , we recover the result in Eqn. 4.

### Appendix C: Calculation of $\langle r^2 \rangle$ and $\langle t \rangle$

Estimates for  $\langle r^2 \rangle$  and  $\langle t \rangle$  are obtained by direct integration over the distribution of outgoing molecular velocities for an emitted molecule

$$P(\vec{v}) d^3\vec{v} = \frac{\cos\theta}{2\pi v_T^4} v \exp\left(-\frac{v^2}{2v_T^2}\right) (v^2 dv d\Omega) \quad (\text{C1})$$

where  $\theta$  and  $\phi$  are the polar and azimuthal emission angles. For both calculations, we divide the distribution into a range of polar angles  $\theta$  (see Fig. 9) for which a molecule emitted from the center of a TM face strikes the opposing cylinder ( $\theta < \theta_c$ ) and another for which the molecule escapes the gap directly ( $\theta > \theta_c$ ), with the critical angle defined by the aspect ratio,  $\tan\theta_c \equiv \frac{R}{d}$ .

For the average time of flight, we obtain

$$\begin{aligned} \langle t \rangle &= \int_{\cos\theta_c}^1 P(v, \theta) \frac{d}{v \cos\theta} v^2 dv d\Omega \\ &\quad + \int_0^{\cos\theta_c} P(v, \theta) \frac{R}{v \sin\theta} v^2 dv d\Omega \\ &= \left(\frac{\pi}{2}\right)^{1/2} \frac{d}{v_T} \left[1 + \frac{R}{d} \left(1 - \sqrt{1 + \left(\frac{d}{R}\right)^2}\right)\right] \\ &\approx \left(\frac{\pi}{2}\right)^{1/2} \frac{d}{v_T} \left(1 - \frac{d}{2R}\right). \end{aligned} \quad (\text{C2})$$

For the calculation of  $\langle r^2 \rangle$  only the angular distribution  $P(\theta, \phi) d\Omega = \frac{1}{\pi} \cos\theta d\Omega$  is relevant. We note that those

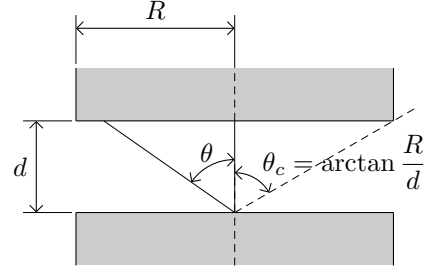


FIG. 9: Illustration of the geometry used for calculating the mean square lateral displacement and the mean time of flight for a molecule emitting into the gap from the center of one of the cylinders. The angle  $\theta_c$  represents the critical value of the polar angle  $\theta$ , beyond which emission from the center results in the molecule escaping the gap laterally in a single flight.

molecules, emitted for  $\theta > \theta_c$ , that directly leave the gap on a single jump from the center are weighted with a lateral displacement that is “saturated” to be  $R$ . We obtain

$$\begin{aligned} \langle r^2 \rangle &= \int_{\cos\theta_c}^1 P(\theta, \phi) d^2 \tan^2\theta d\Omega \\ &\quad + \int_0^{\cos\theta_c} P(\theta, \phi) R^2 d\Omega \\ &= d^2 \ln \left[1 + \left(\frac{R}{d}\right)^2\right]. \end{aligned} \quad (\text{C3})$$

We note that while the average time of flight remains finite for cylinders of infinite radius –  $\langle t \rangle \rightarrow \left(\frac{\pi}{2}\right)^{1/2} \frac{d}{v_T}$ , as we use in the approximate calculation (Eqn. 12) – the mean square displacement diverges, albeit slowly, as  $R/d \rightarrow \infty$ . Saturating the maximum displacement to  $R$  makes physical sense and corresponds to the case of escape on a single bounce. The logarithmic dependence of  $\langle r^2 \rangle$  is a fundamental difference with the result of Ref. [8], where the relevant random walk step size is taken to be  $\langle r \rangle \approx \frac{\pi d}{2}$  (and not the RMS  $\sqrt{\langle r^2 \rangle}$  as used here). This would result in analogous expressions for  $N$ ,  $\tau$ , and  $S_F$  similar to those expressed here (Eqns. 13-19) but without the logarithmic factor. The logarithmic factor, also relevant to similar expressions for the molecular flow impedances of short pipes (for example Ref. [27]) is responsible for the nearly power law dependence of  $\beta$  (or  $S_F$ ) on  $1/d$ , with an exponent that is not exactly 2, but rather approaches 2, from below, only for vanishing gap, as observed here and in the three other numerical and experimental studies cited here (Refs. [5, 6, 8]).

### Acknowledgments

The authors would like to thank Norna Robertson and Jim Hough for stimulating interest in the gas damping

problem for Advanced LIGO. We also thank David Shoemaker and Ray Frey for reviewing the manuscript. LIGO was constructed by the California Institute of Technology and Massachusetts Institute of Technology with funding from the National Science Foundation and operates under cooperative agreement PHY-0757058. The contribution from the Università di Trento was supported by the

INFN, ASI (LISA Pathfinder contract), and the Italian Ministry of University and Research (PRIN 2008). The contribution from the group at the University of Washington was supported by NASA grant NNX08AY66G, by NSF grant PHY0969488, and by DOE funding for the CENPA laboratory. This article has been assigned LIGO document number p1100093.

- 
- \* Current address: Museo delle Scienze, 38122 Trento, Italy
- † Current address: Imperial College, London, UK
- ‡ Current address: National Institute of Standards and Technology, Gaithersburg, Maryland 20899, USA
- [1] R. G. Christian, *Vacuum* **16**, 175 (1966).
- [2] V. B. Braginsky, V. P. Mitropov, and V. I. Panov, *Systems with Small Dissipation* (University of Chicago Press, Chicago, 1985).
- [3] P. R. Saulson, *Phys. Rev. D* **42**, 2437 (1990).
- [4] A. Cavalleri et al., *Phys. Lett. A* **374**, 3365 (2010).
- [5] A. Cavalleri et al., *Phys. Rev. Lett.* **103**, 140601 (2009).
- [6] S. Schlamminger, C. A. Hagedorn, and J. H. Gundlach, *Phys. Rev. D* **81**, 123008 (2010).
- [7] M. Bao and H. Yang, *Sens. Actuators A* **136**, 3 (2007).
- [8] M. Suijlen, J. J. Koning, M. A. J. van Gils, and H. C. Beijerinck, *Sens. Actuators A* **156**, 171 (2009).
- [9] G. M. Harry, *Class. Quant. Grav.* **27**, 084006 (2010).
- [10] Advanced LIGO Team, *Tech. Rep. LIGO-M060056-v2*, LIGO Laboratories, <https://dcc.ligo.org/cgi-bin/DocDB/ShowDocument?docid=m060056> (2011).
- [11] J. K. Fremerey, *J. Vac. Sci. Technol. A* **3**, 1715 (1985).
- [12] S. Dittmann, B. E. Lindenau, and C. R. Tilford, *J. Vac. Sci. Technol. A* **7**, 3356 (1989).
- [13] G. Comsa and R. David, *Surface Science Reports* **5**, 145 (1985).
- [14] A. Cavalleri et al., *Class. Quant. Grav.* **26**, 094017 (2009).
- [15] S. Schlamminger et al., *AIP Conf. Proc.* **873**, 151 (2006).
- [16] S. J. Waldman and the LIGO Scientific Collaboration (2011), *gr-qc/1103.2728v1*.
- [17] N. A. Robertson and J. Hough, *Tech. Rep. LIGO-T0900416-v2*, LIGO, <https://dcc.ligo.org/cgi-bin/DocDB/ShowDocument?docid=T0900416> (2009).
- [18] A. Schram, *Le Vide* **18**, 55 (1963).
- [19] G. Lewin, *Fundamentals of Vacuum Science and Technology* (McGraw-Hill, New York, 1965).
- [20] Virgo Collaboration, *Tech. Rep. VIR-027A-09*, <https://tds.ego-gw.it/ql/?c=6589> (2009).
- [21] K. Arai et al., *Class. Quant. Grav.* **26**, 204020 (2009).
- [22] K. Kuroda and the LCGT Collaboration, *Class. Quant. Grav.* **27**, 084004 (2010).
- [23] ET Science Team, *Tech. Rep. ET-0106C-10*, <https://tds.ego-gw.it/ql/?c=7954> (2011).
- [24] Kazuhiro Yamamoto and the LCGT collaboration, private communication.
- [25] L. W. Bruch, M. W. Cole, and E. Zaremba, *Physical Adsorption: Forces and Phenomena* (Dover, Mineola, New York, 1997).
- [26] G. Vidali, G. Ihm, H. Y. Kim, and M. W. Cole, *Surface Science Reports* **12**, 135 (1991).
- [27] R. G. Livesey, *Vacuum* **76**, 101 (2004).
- [28] In practice, the data for  $S_{F_0}$  in Fig. 3 have been extracted directly from the scatter in the momentum in dedicated long simulations at fixed  $T_0 = 10$  s for many values of  $d$ , using the limit of Eqn. 4 for  $T_0 \gg \tau$ ,  $S_{F_0} = \frac{2\langle(\Delta q)^2\rangle}{T_0}$ .
- [29] Here, however, we insert into Eqn. 14 the “exact” expression for  $\langle t \rangle$ , calculated in Appendix C. This is relevant only at the largest values of  $d$ , where the random walk picture starts to break down, anyways.
- [30] The expression for the torque damping coefficient for a plate of width  $a$ , height  $b$  and thickness  $t$ , can be found by simple integration of the force noise per unit area on the six faces of the prism, following Eqn. 14 in [4]. In the limit of vanishing prism thickness ( $t \ll a$ ), valid to better than 5% for the geometries considered here[6],  $\beta_{rot} = \frac{\rho}{\nu_T} \left(\frac{1}{18\pi}\right)^{1/2} ba^3 \left(1 + \frac{\pi}{4}\right)$ .
- [31] The quantum noise estimate in Ref. [16] differs slightly from that shown in Fig. 8, due to slightly different choice of tunable interferometer detection parameters.
- [32] Even in the infinite volume limit, there is a small decrease in noise at frequencies above  $\tau_{st}^{-1}$ , as the correlation between the momentum exchange from the arrival and re-emission of a molecule striking the TM surface disappears on such timescales. For the Advanced LIGO TM, the reduction is roughly 20%, see Table 1 and Section 2.1.1 of Ref. [4]
- [33] Our analysis differs slightly here from that of Ref. [25] in that we lump their probability of sticking ( $s$ , pg. 110) into the sticking time to form a single sticking time which represents the average time that a molecule spends, per collision, on the surface.